1-1-2005

Theoretical study of dissociative recombination of C-2v triatomic ions: Application to H2D+ and D2H+

Viatcheslav Kokoouline
University of Central Florida

Chris H. Greene

Theoretical study of dissociative recombination of C_{2v} triatomic ions: Application to H_2D^+ and D_2H^+

Viatcheslav Kokoouline
Department of Physics, University of Central Florida, Orlando, Florida 32816, USA

Chris H. Greene
Department of Physics and JILA, University of Colorado, Boulder, Colorado 80309-0440, USA

(Received 16 March 2005; published 17 August 2005)

We develop a theoretical treatment of the dissociative recombination of triatomic molecular ions of the C_{2v} molecular symmetry group. Using the method, we study the dissociative recombination of the H_2D^+ and D_2H^+ ions. The theoretical rates obtained for the H_2D^+ and D_2H^+ dissociative recombination are in general agreement with storage-ring experiments although there are some potentially informative discrepancies.

DOI: 10.1103/PhysRevA.72.022712 PACS number(s): 34.80.Ht, 34.80.Kw, 34.80.Lx

I. INTRODUCTION

The dissociative recombination (DR) of small polyatomic ions is an important process in chemistry of interstellar clouds, planetary atmospheres, and many laboratory experiments. Driven by its importance, significant headway has been achieved in experimental study of the process. Results of astrophysical observations [1–7] and laboratory experiments [8–14] require theoretical interpretation. Such a theoretical description of DR has previously been successful in diatomic ions [15–22]. Some of the principal techniques that have contributed to these successes are multichannel quantum defect theory and the theory of the rovibrational frame transformation [23–26].

In contrast to DR in diatomics, DR in triatomic ions remains a difficult problem for theory. A well-known example is the dissociative recombination of the H_3^+ ion with the electron,

$$H_3^+ + e^- \rightarrow H_2 + H \text{ or } H + H + H.$$

It has been viewed as a particularly important process because H_3^+ is the simplest triatomic ion. But despite its simplicity, DR of H_3^+ has remained an unsolved theoretical problem throughout the past two decades. Important theoretical progress was achieved by Orel and Kulander [27], who developed an understanding of the H_3^+ DR rate at high (6–20 eV) electron-ion collision energy. Later, Schneider *et al.* [28] tried to explain the low-energy range (10^{-3}–6 eV). While this study was crucial in demonstrating the role of indirect Rydberg pathways, the theoretical rate calculated in that study was still orders of magnitude smaller than the measured rate [8].

Recently, we have developed a first-principles theoretical method [29,30] that successfully described the total rate for dissociative recombination of the H_3^+ ion by electron impact, as observed in low-energy storage-ring experiments [8,12,13,31]. The method explains the relatively high DR rate in H_3^+ at low energies (10^{-3}–2 eV), but it involves a number of different and sometimes complicated techniques that accurately represent all degrees of freedom present in the system. However, the key ingredient that proved vital in explaining the unexpectedly high DR rate at these energies is probably not the method itself. We have found that the Jahn-Teller effect [32], which couples electronic and vibrational degrees of freedom, generates the large DR rate in H_3^+. This effect was not incorporated in previous theoretical work [28,33], which is presumably the main reason why previous studies obtained a very low rate.

As a first step in the development of a theoretical approach to the DR process and before we had formulated our most complete quantitative method [29,30], we first devised a simplified approach [32] that successfully accounts for the average enhancement produced by the Jahn-Teller effect. Following our first application of the simplified approach, we also obtained a smaller DR rate (by about a factor of 10). However, it later became clear that the DR rate presented in that work required a correction by a factor of approximately π^2 [34]. With this correction, the theoretical DR rate obtained in that simplified method comes very close to the average experimental rate. Therefore, while the second, more complicated method allows for a more detailed prediction of energy dependences at the resonance-by-resonance level, it is primarily the inclusion of Jahn-Teller coupling physics that plays a crucial role in successfully understanding the high H_3^+ DR rate.

However, the method that we have developed [29,30] is quite general and can be used for the theoretical treatment of other triatomic ions. The second target ion that we considered was D_3^+. It has the same molecular symmetry group D_{3h} and, therefore, can be treated in a similar way: To adapt the method to the D_3^+ ion, only minimal changes had to be introduced. The principal change was to account for the different nuclear spin statistics of deuterium [30]. The theoretical DR rate obtained for D_3^+ is a factor of 2–4 smaller than that for H_3^+, which is in reasonably good agreement with storage-ring experiments [10,35].

The existence of two other isotopomers of H_3^+—i.e., H_2D^+ and D_2H^+—and the corresponding experimental data [8,10] suggests that a further, nontrivial test of the theory is to adapt it to describe ions belonging to the C_{2v} molecular symmetry group. Fortunately, we can use the same ionic Born-Oppenheimer potential surface for all four isoto-

pomers, since the surface is calculated in the approximation of infinite masses of the three nuclei. In addition, the molecular potential is very well known for H_3^+ [36,37], which is not the case for many other triatomic ions of interest. In the experiments, the DR rate for the four isotopomers is different. (For example, the 300 K H_3^+ DR rate is 4 times larger than the D_3^+ DR rate.) Therefore, the different H_3^+ isotopomers provide a unique opportunity to develop and test the method, which after refinement can hopefully be applied to other triatomic ions.

The goal of the present study is to adapt our method to treat triatomic ions of the C_{2v} symmetry group and apply it to a first test case of dissociative recombination for the H_2D^+ and D_2H^+ ions.

The article is organized as following. In the next section we describe our theoretical method. Since the method was already presented in a previous publication [30], we discuss here only the part of the method that is different for C_{2v} ions. Section III presents a test of the accuracy of the adiabatic hyperspherical approach employed earlier for H_3^+ and D_3^+. Since the adiabatic approximation did not reproduce the vibrational spectrum of H_2D^+ and D_2H^+ sufficiently well, we have developed an improved treatment of those degrees of freedom. Section III describes that improved treatment. Section IV presents results for the H_2D^+ and D_2H^+ DR rates and a comparison with the experiment. Finally, Sec. V concludes the article. In the Appendix we discuss how experimental conditions must be accounted for in order to directly compare the theoretical DR rate with measured values.

II. THEORY OF THE DISSOCIATIVE RECOMBINATION OF C_{2v} TRIATOMIC IONS

A. Overall symmetry of H_2D^+ and D_2H^+ wave functions

The overall symmetry of H_2D^+ and D_2H^+ was discussed in detail in our earlier study [38]. Here we present only a brief overview of the key aspects.

The molecular symmetry group of the H_2D^+ and D_2H^+ ions in their ground electronic state is C_{2v}. There are four elements in this group [E, (12), E^*, and $(12)^*$] generated by two operations: inversion E^* and permutation (12) of two identical particles ($H \leftrightarrow H$ or $D \leftrightarrow D$).

As in our treatment of the H_3^+ ion, we construct the total wave function of the ion-electron complex as a product of four factors corresponding to rotational, vibrational, electronic, and nuclear spin degrees of freedom,

$$\Phi_{total} = \Phi_{rot}\Phi_{vib}\Phi_{el}\Phi_{ns}. \tag{1}$$

We utilize two full sets (bases) of functions Φ_{total}. One basis $\Phi_{total}^{(l)}$ is adapted for a description of the system at large separations between the electron and ion: it diagonalizes the total Hamiltonian when the electron is far from the ion. The second basis $\Phi_{total}^{(s)}$ corresponds to small electron-ion separations: the short-range Hamiltonian is almost diagonal in this basis.

The allowed symmetries of the total wave function Φ_{total} of H_2D^+ are limited to the B_1 and B_2 irreducible representations of C_{2v} because Φ_{total} must be antisymmetric with respect to (12). For the same reason, the total symmetry of Φ_{total} of D_2H^+ can be A_1 or A_2.

B. Symmetry of vibrational, rotational, nuclear-spin, and electronic wave functions

1. Rotational wave functions

The rotational part $\Phi_{rot}^{(l)}$ and $\Phi_{rot}^{(s)}$ of the total wave function is constructed in the $\Phi^{(l)}$ and $\Phi^{(s)}$ bases in a similar way.

The ions H_2D^+ and D_2H^+ are asymmetric tops. Therefore, the rotational wave functions are obtained by a diagonalization of the well-known rotational Hamiltonian of the asymmetric top:

$$H_{rot} = B^{(1)}\hat{N}_1^2 + B^{(2)}\hat{N}_2^2 + B^{(3)}\hat{N}_3^2. \tag{2}$$

In the above equation, $\hat{N}_i$ are the three angular momentum operators projected onto the principal axes of inertia of the molecule and $B^{(i)}$ are rotational constants related to the three principal moments of inertia. Since the three nuclei lie in a plane, one axis of inertia is perpendicular to that plane and the corresponding moment of inertia is the sum of the two other moments. The constants $B^{(i)}$ depend on the vibrational state.

Matrix elements of H_{rot} of different terms in Eq. (2) are reasonably simple in the basis of symmetric top rotational wave functions

$$\mathcal{R}^{N^+}_{k^+m^+}(\alpha,\beta,\gamma) = \left[\frac{2N^+ + 1}{8\pi^2}\right]^{1/2} [D^{N^+}_{m^+,K^+}(\alpha,\beta,\gamma)]^* \tag{3}$$

and given, for example, in [39] (see also our article [38]).

Eigenstates of the matrix H_{rot}, asymmetric top rotational functions, are classified by four quantum numbers. These are the total angular momentum N, its projection on a laboratory-fixed axis, m, the parity $p_1^{(rot)} = \pm 1$, and the eigenvalue $p_2^{(rot)}$ with respect to (12), $p_2^{(rot)} = \pm 1$. We will reference to the resulting eigenstates of the asymmetric top as $|N,m,p_1^{(rot)},p_2^{(rot)}\rangle$.

The symmetry properties of $|N,m,p_1^{(rot)},p_2^{(rot)}\rangle$ are discussed in more detail in Ref. [38].

2. Electronic wave functions

As in our previous study of H_3^+ DR, we consider here only the np-electron states, because these are the states predominantly relevant to the dissociative recombination experiments. The electronic states are constructed in a different way for $\Phi_{total}^{(s)}$ and $\Phi_{total}^{(l)}$ [29,30,40–44]. The electronic wave function $\Phi_{el}^{(s)}$ is given by a spherical harmonic $Y_{1,\Lambda}(\theta,\phi)$, where Λ is the projection of the electronic orbital momentum $l=1$ on the molecular axis of symmetry and the angles θ and ϕ are spherical coordinates of the electron with respect to the molecule-fixed coordinate system. The electronic wave function $\Phi_{el}^{(l)}$ is also a spherical harmonic $Y_{1,\lambda}(\theta',\phi')$, where λ is now the projection on the laboratory z axis and the angles θ' and ϕ' refer to the laboratory coordinate system.

The spherical harmonics $Y_{1,\Lambda}(\theta,\phi)$ and $Y_{1,\lambda}(\theta',\phi')$ do not transform according to a definite irreducible representa-

tion of the C_{2v} symmetry group. In order to obtain electronic functions belonging to a definite irreducible representation, we form appropriate linear combinations of the spherical harmonics: Using their symmetry properties, we obtain [38] electronic wave functions $\Phi_{el}^{(s)}$:

$$\Gamma = A_1: Y_{1,X}(\theta,\phi) = \frac{1}{\sqrt{2}}[Y_{1,1}(\theta,\phi) + (-1)^1 Y_{1,-1}(\theta,\phi)],$$

$$\Gamma = B_1: Y_{1,Z}(\theta,\phi) = Y_{1,0}(\theta,\phi),$$

$$\Gamma = B_2: Y_{1,Y}(\theta,\phi) = \frac{1}{i\sqrt{2}}[Y_{1,1}(\theta,\phi) - (-1)^1 Y_{1,-1}(\theta,\phi)]. \tag{4}$$

For $\Phi_{el}^{(l)}$, the operator (12) is not diagonal because $Y_{1,\lambda}(\theta',\phi')$ is a mixture of the three different $Y_{1,\Lambda}(\theta,\phi)$. The inversion of $\Phi_{el}^{(l)}$ is defined by the familiar formula

$$E^* Y_{1,\lambda}(\theta',\phi') = (-1)^1 Y_{1,\lambda}(\theta',\phi').$$

3. Vibrational wave functions

Since the molecular XY plane is fixed by the plane of the three nuclei, vibrational motion occurs only in that plane, and therefore, the possible irreducible representations of vibrational motion are A_1 and B_2.

The ionic vibrational basis $\Phi_{vib}^{(s)}$ is chosen to be the set of position eigenstates of the vibrational coordinates $\mathcal{Q}$: $\Phi_{vib}^{(s)} = |\mathcal{Q}\rangle$, where $\mathcal{Q}$ denotes three hyperspherical coordinates. The vibrational state $\Phi_{vib}^{(l)}$ is given by the vibrational quantum number $\mathcal{V}$ of the ion: $\Phi_{vib}^{(l)} = |\mathcal{V}\rangle$. The transformation coefficients connecting the two vibrational bases are given by

$$\langle \Phi_{vib}^{(l)} | \Phi_{vib}^{(s)} \rangle = \langle \mathcal{V} | \mathcal{Q} \rangle = \chi_{\mathcal{V}}(\mathcal{Q}), \tag{5}$$

which coincide with ionic vibrational eigenfunctions.

4. Nuclear spin wave functions

The spin eigenfunctions Φ_{ns} are unchanged by the operator E^* of the coordinate inversion. Therefore, the allowable irreducible representations for Φ_{ns} are A_1 and B_2. The nuclear states of two identical nuclei are specified by their spins i and spin projections m_i, with $i=1/2$ for H_2D^+ and $i=1$ for D_2H^+. The nuclear spin irreducible representation—i.e., A_1 or B_2—is determined by the factor $(-1)^{i_1+i_2-I}$. For A_1 it is +1; for B_2 it is −1 [38]. The nuclear spin wave functions Φ_{ns} are the same in the short- and long-range bases.

C. Jahn-Teller coupling in H_2D^+

As in our treatment of H_3^+ DR, we introduce the physics of Jahn-Teller coupling using the reaction matrix $K_{s,s'}$ (see Refs. [43–47]). Since the reaction matrix for H_3^+ [30] is obtained in the Born-Oppenheimer approximation, it can also be used in other isotopomers of H_3^+. However, the matrix in Ref. [30] must be slightly modified to be used in the basis of electronic states Y_{1j} ($i=X$, Y, or Z) since the initial K matrix is defined in the basis of $Y_{1\Lambda}$. The resulting reaction matrix is

$$K_{i,i'}(\mathcal{Q}) = \begin{pmatrix} \tan[\pi\mu_{\Lambda=0}(\mathcal{Q})] & 0 & 0 \\ 0 & \delta\rho^2 - \lambda\rho\cos(\phi) & -\lambda\rho\sin(\phi) \\ 0 & -\lambda\rho\sin(\phi) & \delta\rho^2 + \lambda\rho\cos(\phi) \end{pmatrix}. \tag{6}$$

D. Hyperspherical coordinates for C_{2v} molecules: Principal moments of inertia

For the H_2D^+ and D_2H^+ ions, the hyperspherical coordinates adopted are defined differently than in H_3^+, because the three nuclear masses are unequal. The three hyperspherical coordinates R, $\varphi^{(h)}$, and $\theta^{(h)}$ can be defined through the three internuclear distances $|\vec{r}_{12}|$, $|\vec{r}_{23}|$, and $|\vec{r}_{31}|$ as [48]

$$|\vec{r}_{23}| = \frac{Rd_1}{\sqrt{2}}\sqrt{1+\sin\theta^{(h)}\sin\varphi^{(h)}},$$

$$|\vec{r}_{31}| = \frac{Rd_2}{\sqrt{2}}\sqrt{1+\sin\theta^{(h)}\sin(\varphi^{(h)}-\epsilon_2)},$$

$$|\vec{r}_{12}| = \frac{Rd_2}{\sqrt{2}}\sqrt{1+\sin\theta^{(h)}\sin(\varphi^{(h)}+\epsilon_3)}, \tag{7}$$

where

$$\epsilon_2 = 2\arctan(m_3/\mu),$$

$$\epsilon_3 = 2\arctan(m_2/\mu),$$

$$d_i = \sqrt{(m_i/\mu)(1-m_i/M)},$$

$$M = m_1 + m_2 + m_3,$$

$$\mu = \sqrt{m_1 m_2 m_3/M}. \tag{8}$$

m_1, m_2, and m_3 are masses of the three nuclei in the ion. For the H_2D^+ and D_2H^+ ions, two masses of the three are the same. The hyperradius R can vary in the interval $[0,\infty)$, the hyperangle $\varphi^{(h)}$ varies over $[0,2\pi)$, and $\theta^{(h)}$ varies over the interval $[0,\pi/2]$.

Since each of these ions is an asymmetric top molecule, we also need expressions for the rotational constants $B_{\mathcal{V}}^{(i)}$ in Eq. (2). These are given by [48]

$$B_{\mathcal{V}}^{(i)} = \langle \mathcal{V} | 1/(2I_i) | \mathcal{V} \rangle, \tag{9}$$

where I_i are principal moments of inertia. In hyperspherical coordinates the expressions are

$$I_1 = \frac{1}{2}\mu R^2(1-\sin\theta^{(h)}),$$

$$I_2 = \frac{1}{2}\mu R^2(1+\sin\theta^{(h)}),$$

$$I_3 = I_Z = I_1 + I_2 = \mu R^2. \quad (10)$$

The integration $\langle\|\rangle$ in Eq. (9) is made over all three hyperspherical coordinates.

E. Frame transformation

The final scattering matrix for electron-ion collisions is obtained using a frame transformation between wave functions $\Phi^{(l)}_{total}$ describing the system at large electron distances r and wave functions $\Phi^{(s)}_{total}$ describing the system at small r. The final scattering matrix has a form similar to the one derived for H_3 [Eq. (42) of Ref. [30]],

$$\mathcal{S}^{(l)} = \mathcal{U}\mathcal{S}^{(s)}\mathcal{U}^{\dagger}, \quad (11)$$

where the matrix elements $\mathcal{U}_{l,s}$ of the rovibrational frame transformation are given by inner products:

$$\mathcal{U}_{l,s} = \langle \Phi^{(l)}_{total} | \Phi^{(s)}_{total} \rangle.$$

A difference from the H_3^+ treatment is in the rotational coefficients $\langle \Phi^{(l)}_{rot}\Phi^{(l)}_{el} | \Phi^{(s)}_{rot}\Phi^{(s)}_{el} \rangle$. In the present study, they are not just Clebsch-Gordan coefficients $C^{N^+,k^+}_{l,-\Lambda;N,k}$ as was the case for H_3^+ [30], because the rotational functions for H_2D^+ and D_2H^+ are not symmetric top eigenstates and the electronic functions $Y_{1,X}$ and $Y_{1,Y}$ are not pure spherical harmonics. The rotational frame transformation coefficients $\langle \Phi^{(l)}_{rot}\Phi^{(l)}_{el} | \Phi^{(s)}_{rot}\Phi^{(s)}_{el} \rangle$ can be obtained using a sequence of unitary transformations: (i) The coefficients linking asymmetric top functions $|\Phi^{(l)}_{rot}\rangle$ with symmetric top functions $\mathcal{R}^{N^+}_{k^+m^+}$ are obtained from a diagonalization of the rotational Hamiltonian of Eq. (2). (ii) The electronic functions $Y_{1,X}$ and $Y_{1,Y}$ are linked to spherical harmonics by Eq. (4). (iii) The unitary transformation between ionic and neutral-molecule symmetric top functions is performed using Clebsch-Gordan coefficients $C^{N^+,k^+}_{l,-\Lambda;N,k}$ [Eq. (41) of Ref. [30]]. (iv) Finally, the transformation from symmetric top functions $\mathcal{R}^{N}_{km}$ to asymmetric top functions $|\Phi^{(s)}_{rot}\rangle$ is carried out in a manner very similar to (i).

F. Scattering matrix and the DR cross section and rate

To obtain the matrix $\mathcal{S}^{(l)}_{l',l}$, where subscripts l and l' refer to possible channels $\Phi^{(l)}$ of $\mathcal{S}^{(l)}$, we use Eq. (11). For this, we first calculate the scattering matrix $\mathcal{S}^{(s)}$ in the short-separation states $\Phi^{(s)}$. The matrix $\mathcal{S}^{(s)}$ is obtained using the short-separation reaction matrix of Eq. (6). The transformation $K_{ii'} \rightarrow \mathcal{S}^{(s)}_{l',l}$ is performed using the standard quantum defect procedure [for example, see Eq. (2.43) in [25]].

The vibrational state $\Phi_{vib}(\mathcal{Q})$ can be either a bound or continuum wave function. The scattering matrix $\mathcal{S}^{(l)}$ obtained is not unitary because it contains information about the dissociation: Not all the incoming electron flux eventually ends up in the outgoing flux. A fraction of the flux goes into dissociative channels.

The calculated energy-independent scattering matrix $\mathcal{S}^{(l)}$ is then used to obtain the physical scattering matrix $\mathcal{S}^{phys}(E)$. The DR cross section and rate are then calculated using the defect from unitarity of the relevant columns of the matrix $\mathcal{S}^{phys}(E)$. This aspect of the DR calculation for H_2D^+ and D_2H^+ is the same as for H_3^+ and D_3^+, which was already described in a previous publication (see Sec. VII of Ref. [30]).

III. ACCURACY OF THE VIBRATIONAL EIGENFUNCTIONS

A. Adiabatic hyperspherical approximation and its accuracy

The key idea of the adiabatic hyperspherical approach [49] is to view the hyperradius as a slowly varying coordinate, in contrast to fast-changing hyperangular coordinates. This assumption allowed us to obtain the vibrational eigenenergies E_{vib}, and the corresponding three-dimensional vibrational wave functions $\Phi_{vib}(R,\theta^{(h)},\phi^{(h)})$ is the two-step procedure [29,30]: First, adiabatic hyperspherical curves $U_a(R)$ are obtained by a diagonalization of the fixed-R Hamiltonian, in the two-dimensional hyperangle space,

$$H^{ad}\varphi_a(R_i;\theta^{(h)},\phi^{(h)}) = U_a(R_i)\varphi_a(R_i;\theta^{(h)},\phi^{(h)}). \quad (12)$$

Then, for each adiabatic curve $U_a(R)$, the one-dimensional Schrödinger equation is solved,

$$[K(R) + U_a(R) - E_{a,v}]\psi_{a,v}(R) = 0, \quad (13)$$

where H^{ad} is the vibrational Hamiltonian assuming that the hyperradius R is fixed and $K(R)$ represents the kinetic energy term associated with the hyperradial motion. Correspondingly, the total three-dimensional vibrational wave functions are given in the form

$$\Phi_{vib}(R,\theta^{(h)},\phi^{(h)}) = \psi_{a,v}(R)\varphi_a(R;\theta^{(h)},\phi^{(h)}) \quad (14)$$

in the adiabatic approximation.

Figure 1 shows several adiabatic hyperspherical potential curves $U_a(R)$ of the H_2D^+ and D_2H^+ ions. As one can see the curves for the two ions look very similar.

As we discussed earlier, the adiabatic hyperspherical approximation was good enough to be used in the theoretical treatment of DR in H_3^+. Because of the success we found with this approach for H_3^+ and D_3^+, we initially attempted to use the adiabatic approximation for the two other asymmetric isotopomers of H_3^+. However, test cases showed that the vibrational eigenenergies $E_{a,v}$ calculated for H_2D^+ and D_2H^+ using this approximation are far less accurate than for H_3^+ and D_3^+. The results of the vibrational level calculation for all the four H_3^+ isotopomers using the adiabatic hyperspherical approximation are given in Table I. However, since at that time we did not have a better way to represent the vibrational eigenstates, we decided to keep the approach and carry out a complete calculation of the DR rate. The resulting DR rate for H_2D^+ was about a factor of 3 larger than the experimental one from the CRYRING storage ring [35]. The theoretical and experimental rates are shown in Fig. 3, below. Such a big difference between calculation and the experiment could potentially mean that the quality of the vibrational eigenfunctions is not satisfactory. This difficulty has led us to improve the vibrational energy level calculation and to go beyond the adiabatic hyperspherical approximation for DR in H_2D^+ and D_2H^+.

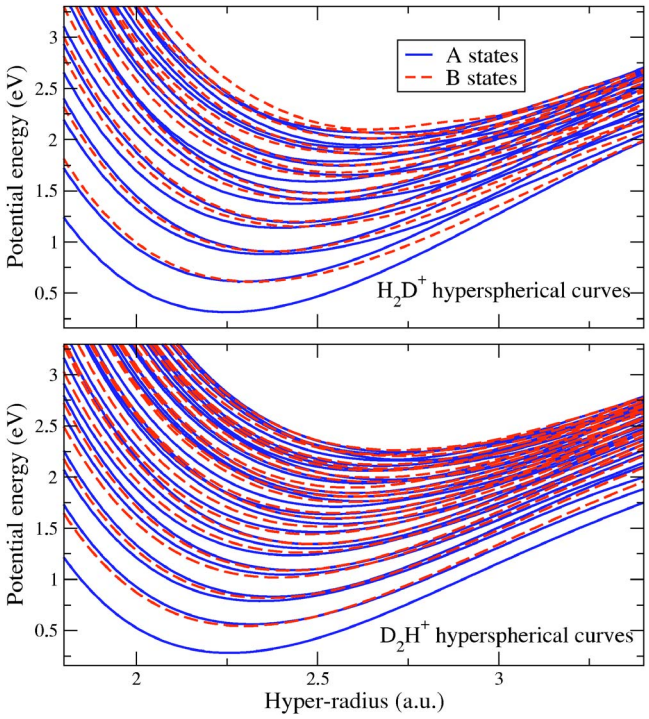

FIG. 1. (Color online) Several first adiabatic hyperspherical potential curves for the H_2D^+ ion (upper panel) and for the D_2H^+ ion (lower panel). The curves can be classified according to one of the two A or B irreducible representations of the vibrational symmetry group.

B. Slow variable representation

Although the adiabatic hyperspherical approach failed, the hyperspherical coordinates are still attractive for the DR treatment, because the hyperradius naturally represents the dissociation coordinate. The slow variable discretization (SVD) method proposed by Tolstikhin *et al.* [52] suggests that we might be able to retain the hyperradius as the dissociation coordinate and, simultaneously, to calculate and utilize essentially exact vibrational eigenfunctions.

The original detailed description of the SVD method was presented in Ref. [52]. Our treatment slightly modifies the method, as is briefly described below. In the first step, the adiabatic eigenenergies $U_a(R_i)$ and eigenfunctions $\varphi_a(R_i;\theta^{(h)},\phi^{(h)})$ at a fixed hyperradius R_i are obtained on a grid of R_i values by solving the same eigenvalue equation (12) as in the adiabatic approach.

In the second step, the exact vibrational eigenstate $\Phi_{vib}(\mathcal{Q})$ is represented as an expansion in the basis of the functions $\varphi_a(R_i;\theta^{(h)},\phi^{(h)})$. The coefficients of expansion $\psi_a(R_i)$ depend on the hyperradius R_i:

$$\Phi_{vib}(\mathcal{Q}) = \sum_a \psi_a(R_i)\varphi_a(R_i;\theta^{(h)},\phi^{(h)}). \tag{15}$$

The hyperradial wave functions $\psi_a(R_i)$ in their turn are expanded in the discrete variable representation (DVR) basis $\pi_j(R)$ [52]:

$$\psi_a(R) = \sum_j c_{j,a}\pi_j(R). \tag{16}$$

In our version of the treatment, we use B splines instead of the DVR basis. After inserting the two above expansions into the original vibrational eigenvalue problem $H\Phi_{vib}(\mathcal{Q}) = E\Phi_{vib}(\mathcal{Q})$, we obtain

$$\sum_{i',a'} [\langle\pi_{i'}|K(R)|\pi_i\rangle\mathcal{O}_{i'a',ia} + \langle\pi_{i'}|U_a(R)|\pi_i\rangle\delta_{a'a}]c_{i'a'} = E\sum_{i',a'}\langle\pi_{i'}|\pi_i\rangle\mathcal{O}_{i'a',ia}c_{i'a'}, \tag{17}$$

with $\mathcal{O}_{i'a',ia}$

$$\mathcal{O}_{i'a',ia} = \langle\varphi_{a'}(R_{i'};\theta^{(h)},\phi^{(h)})|\varphi_a(R_i;\theta^{(h)},\phi^{(h)})\rangle. \tag{18}$$

In Eq. (17), on the right-hand side, the overlap matrix element $\langle\pi_{i'}|\pi_i\rangle$ appears because the B-spline representation basis is not orthogonal.

Equation (17) is a generalized eigenvalue problem for the eigenvalues E and corresponding eigenvectors $\vec{c}$, and it can be solved using standard numerical procedures.

Table II compares eigenenergies obtained using the SVD method with the exact energies obtained in Ref. [51]. Figure 2 demonstrates the multichannel wave function for the first exited vibrational level $v_A=1$, $(v_1v_2v_3)=(010)$, $E=2205.2$ cm^{-1} of the A symmetry. As one can clearly see,

TABLE I. Several vibrational energies of the H_2D^+ and D_2H^+ ions in cm^{-1}. The first number in each cell of the table gives the energy obtained in the present study using the adiabatic hyperspherical approximation; the second number in a cell gives the actual energy of the state.

$(v_1v_2^{l_2})$, D_{3h}	H_3^+	D_3^+	$(v_1v_2v_3)$, C_{2v}	H_2D^+	D_2H^+
(10^0)	3188	2306	(100)	2781	2431
	3178.5[a]	2301.36[b]		2992.51[c]	2736.98[c]
(01^1)	2516	1833	(010)	2382	2210
	2521.20[a]	1834.67[c]		2205.87[c]	1968.17[c]
(02^2)	5001	3650.8	(001)	2328	2086
	4997.73[a]	3650.55[b]		2335.45[c]	2078.43[c]

[a]Reference [37].
[b]Reference [50].
[c]Reference [51].

TABLE II. Several vibrational energies of the H_2D^+ calculated using the adiabatic hyperspherical approximation and SVD method. For a comparison, the exact energies [51] are also given.

Symmetry $(v_1v_2v_3)$	Adiabatic energies	SVD energies	Exact calc.
A (000)	0	0	0
A (100)	2781	2993.8	2992.51
A (010)	2328	2205.2	2205.87
B (001)	2382	2335.2	2335.45

contributions from the first two channels $a=1,2$ are comparable. The contribution from the third channel is also not negligible. The non-negligible contribution from several adiabatic channels a explains why the accuracy of the adiabatic approximation is so poor.

Therefore, in the current DR treatment of H_2D^+ and D_2H^+ we use the hyperspherical coordinates and the SVD method to represent and calculate the vibrational eigenfunctions and eigenenergies.

C. Vibrational eigenfunction of the continuum spectrum and the complex absorbing potential

As in the DR treatment of H_3^+ and D_3^+ we need not only the bound vibrational eigenfunctions but also the continuum eigenfunctions. Using the adiabatic approximation we obtained the continuum wave functions applying another method suggested by Tolstikhin *et al.* [53,54]: namely, the Siegert state method. However, it appears as though the method cannot be used in a general multichannel problem until or unless it is generalized further. For this reason, we decided to use another approach to determine the continuum eigenfunctions: namely, the complex absorbing potential method. Out of the different versions of this method that are available, we have chosen the one described by Vibok and Balint-Kurti [55,56]. To keep the hyperradial grid of modest extent, we have chosen a quadratic complex absorbing potential that is placed at the end of the grid. The parameters of the absorbing potential were chosen according to the instructions of Ref. [55].

IV. RESULTS FOR THE DR RATES OF H_2D^+ AND D_2H^+

The theoretical DR rate $\alpha(E)$ calculated has hundreds of sharp resonances associated with autoionizing states of the neutral H_2D^+ or D_2H^+ molecule. The data from storage ring experiments do not exhibit such resonances for collision energies below 5 eV. We attribute the absence of resonances in the experimental data to a wide experimental spread in the collision energy. However, we do note that a recent experiment with better resolution [13] does exhibit some resonances for the H_3^+ ion. Thus, to compare our theoretical results with the experimental date we have to average the theoretical DR rate $\alpha^{(raw)}(E)$ over the experimental energy distribution.

There are three distributions that must be considered: (1) the collision energy distribution, (2) the target ion rotational energy distribution, and (3) the toroidal correction. The actual averaging procedure was briefly discussed in a previous publication [34]. Since the procedure was found to be important in order to discern a proper theory-experiment comparison, we give in the Appendix a detailed description of all three averaging procedures.

Figures 3 and 4 present the theoretical DR rate obtained for H_2D^+ and D_2H^+. The first figure (Fig. 3) compares the theoretical H_2D^+ DR rate (solid thick curve) with the experimental data from the CRYRING storage ring experiment of Ref. [35]. The theoretical DR rate shown in the figure includes all averagings described above. The overall agreement

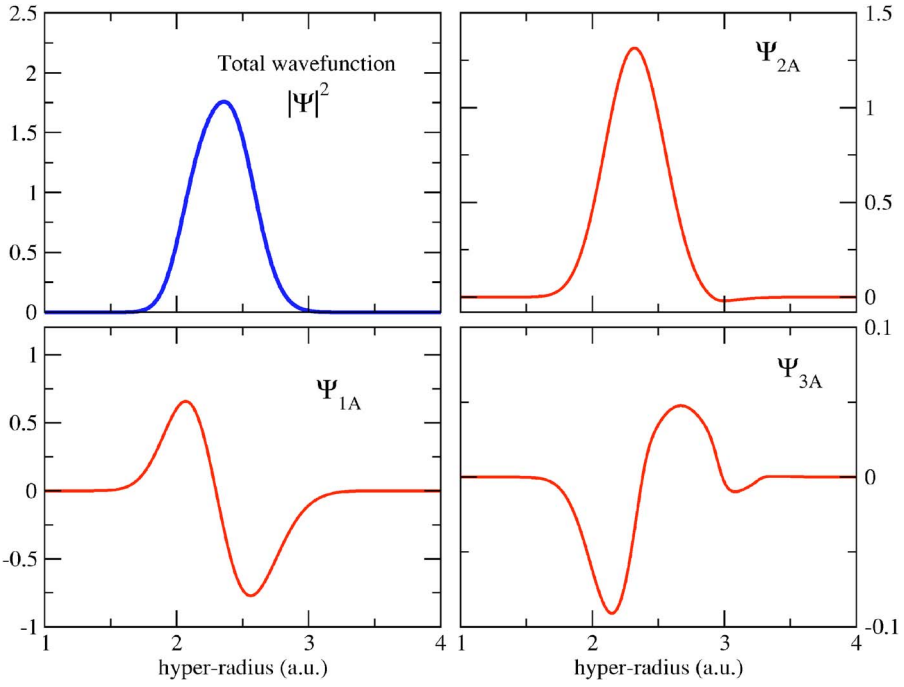

FIG. 2. (Color online) Hyperradial dependence $\psi_a(R)$ of the first excited $(v=1)$ A vibrational wave function of H_2D^+ calculated using the SVD method. In the SVD method, vibrational eigenfunctions are multichannel [see Eq. (15)]. The upper left panel shows the norm of the function summed over all channels; the three other panels show contributions $\psi_a(R)$ of the first three adiabatic channels $(a=1,2,3)$ to the total eigenfunction.

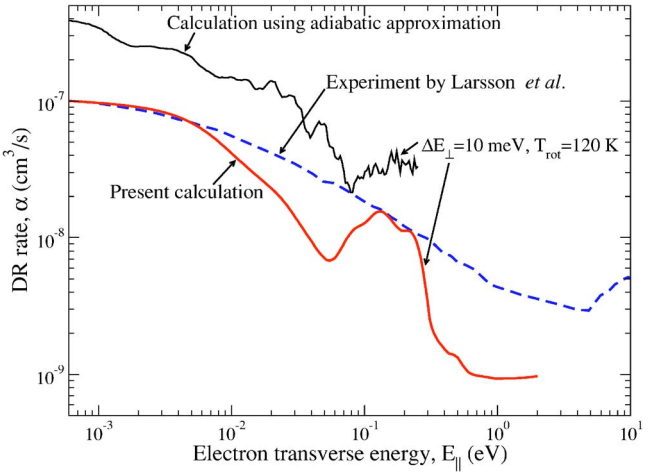

FIG. 3. (Color online) Experimental [35] (dashed curve) and theoretical (thick solid curve) H_2D^+ DR rates. The final theoretical DR rate (thick curve) is averaged according to Eq. (A4). The thin solid line represents the DR rate calculated using the adiabatic vibrational eigenfunctions.

between theory and experiment is good. The theoretical and experimental curves disagree in two energy regions, at 0.01–0.09 eV and 0.3–2 eV, where the theoretical DR is smaller than the experimental one by a factor of 2–5. The reason for the discrepancy in the first region is not yet clear to us. We would like to note that a similar discrepancy is present in the H_3^+ rate (see Fig. 6, below). The second region of discrepancy is probably associated with the toroidal correction. We do not have the exact parameters for the toroidal effect in the experiment of Ref. [35], which would be needed to accurately simulate the toroidal correction to the theoretical DR curve; accordingly, we use the same parameters that we used previously to estimate this effect for H_3^+ [13]. As far as we know, the experimental conditions in Refs. [13,35] may be different. Comparing the two theoretical curves in Fig. 6, below, one can see that the DR rate in the 0.3–2 eV energy region depends sensitively on the actual parameters of toroidal correction. For this reason, we do not believe that the second discrepancy region is a significant concern, as it does not provide unambiguous evidence for problems in our theoretical description of the DR process.

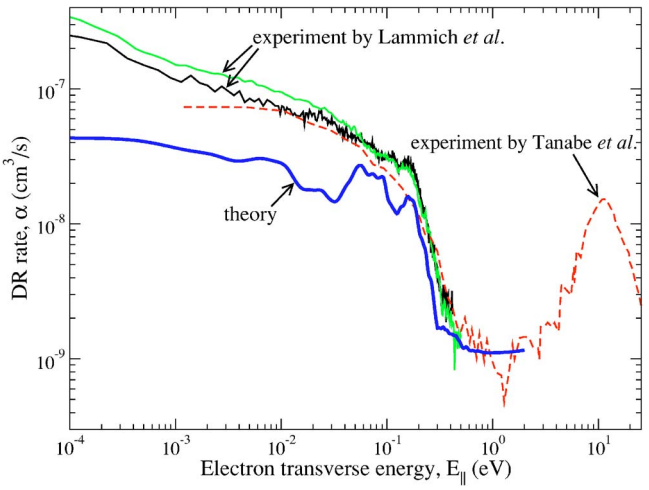

FIG. 4. (Color online) Comparison between theoretical and experimental results for DR rate in D_2H^+. The experimental rates are from Lammich *et al.* [57] and Tanabe *et al.* [10]. The experimental curve from the experiment of Tanabe *et al.* [10] is scaled to obtain the agreement with the experiment of Lammich *et al.* [57] at large (10 eV) collision energy, where Lammich *et al.* measured the DR rate equal to $1.6\pm0.5\times10^{-8}$ cm^3/s. When the averaging was performed on the theoretical curve, we used the three energy distribution widths from Ref. [57]: namely, $\Delta E_{\parallel}=0.07$ meV, $\Delta E_{\perp}=12$ meV, and $T_{rot}=300$ K.

Figure 3 shows also one other theoretical DR rate, calculated using the adiabatic hyperspherical description of the ionic vibrations. We ascribe the considerable difference between the two theoretical curves to the poor accuracy of the vibrational eigenfunctions of H_2D^+ in the adiabatic approximation.

The second figure (Fig. 4) compares our theoretical results (thick solid curve) with the data from two measurements [10,57] (thin dashed and solid curves) of the DR rates for D_2H^+. As in Fig. 3, the theoretical curve includes all averagings discussed above. One experimental curve (the dashed one) is from the TARN II storage ring experiment of Tanabe *et al.* [10], two other experimental curves (thin solid lines) are from the TSR storage ring experiment of Lammich *et al.* [57]. In the experiment of Tanabe *et al.* [10] the measured DR rate is given only in relative units. Thus, we have to scale it by a suitably chosen factor. The scaling we have chosen was based on the assumption that the DR rate at the high-energy peak at 10 eV is roughly the same in the experiment of Lammich *et al.* [57]: At 10 eV, Lammich *et al.* have measured the DR rate to be $1.6\pm0.5\times10^{-8}$ cm^3/s. Experimental data for the averaging parameters are given for the experiment of Lammich *et al.* but unknown for the experiment of Tanabe *et al.* Therefore, the theoretical DR rate was averaged using the parameters from Ref. [57]. The agreement between theory and experiment is reasonably encouraging in the energy range 0.06–2 eV, but at energies below 0.06 eV theory predicts a DR rate that is 2–4 times smaller than the experiment. The reason for this disagreement is not clear.

In Fig. 4 we included two experimental curves from the experiment of Lammich *et al.* [57]. The difference between the curves is in the time during which the D_2H^+ ions were precooled and stored before colliding with electrons. For the lowest curve the precooling time t_p is 30 s and the storage time t is 61 s, while for the upper curve two shorter times were used, $t_p=5$ s and $t=11$ s, respectively [57]. It is not quite clear what experimental curve should be viewed as the one corresponding to the thermal equilibrium. This question merits a separate detailed consideration, which is beyond the scope of the present paper, but we would like to briefly comment on this issue here. The longer precooling time helps to decrease the rotational temperature of the D_2H^+ ions. The rotational temperature is expected to decrease initially, because at the beginning it is known to be much higher than 300 K. The longer storage time t helps to establish a thermal equilibrium of the D_2H^+ ions with the blackbody radiation. In the absence of further, detailed tests, one should not discount the possibility that passage of the ions through the

toroidal region might produce some rotational heating, which would tend to counter the cooling effect of waiting for longer times. Nevertheless, we tend to think that the lower experimental curve better represents the equilibrium with blackbody radiation at 300 K. However, since this issue is not yet completely clear, we have included both experimental curves in the figure.

We note that the higher-resolution experimental curves by Lammich *et al.* show several weak resonances in the region 0.08–0.2 eV. The positions and approximate widths of the resonances appear to be in general agreement with the analogous features in our theoretical curve. These resonances are due to Rydberg states of the neutral molecule D_2H, which belong primarily to the two Rydberg series converging to (010) and (001) vibrational states of the D_2H^+ ion. A similar Rydberg series is visible in the experimental and theoretical DR rate for the H_3^+ ion (Fig. 6, below). In H_3 the Rydberg series are converging to the doubly degenerate $E(01^1)$ vibrational level of the ion. (Any doubly degenerate E vibrational state in H_3^+ corresponds to two vibrational levels in D_2H^+ or H_2D^+; one level is of the A irreducible representation, the other one B.)

V. SUMMARY AND CONCLUSIONS

In the present study we have discussed several issues and developments in the dissociative recombination of triatomic ions.

(i) *Theoretical method for DR in C_{2v} ions*. In this study we have developed an approach to calculate the DR rate for triatomic molecular ions of the C_{2v} molecular symmetry group. The approach is similar to the one developed earlier for ions of the D_{3h} symmetry group but it has a number of important differences.

(ii) *Main differences in the DR treatment of D_{3h} and C_{2v} ions*. One principal difference in the theoretical treatments of the C_{2v} and D_{3h} ions is a different way to construct total wave functions. All four factors—vibrational, rotational, electronic, and nuclear spin—in the total wave function of the ions are constructed differently. This is because the wave functions of the C_{2v} and D_{3h} ions are transforming according to different sets of irreducible representations of the corresponding molecular symmetry group. The second principal difference is in the calculation of the vibrational eigenfunctions of the ions. The adiabatic hyperspherical approach employed for H_3^+ and D_3^+ in our previous study [29,30] is not sufficiently accurate for H_2D^+ and D_2H^+. To improve the accuracy we used the slow variable discretization technique [52]. The resulting vibrational eigenenergies are in excellent agreement with "exact" three-dimensional calculations. Using the SVD technique we had to abandon the Siegert state method that was used for H_3^+ and D_3^+ because it cannot be adapted to multichannel eigenvalue problem. Instead, we have used the method of complex absorbing potential [55,56].

(iii) *Accounting for experimental conditions*. In the present study we have accounted for several experimental effects present in the storage ring experiment. Not all these effects were not accounted for in our initial studies [29,30] of DR in H_3^+ and D_3^+. Once they have been included, the agreement between theory and experiment for H_3^+ is significantly improved (Fig. 6, below).

(iv) *Results for the H_2D^+ and D_2H^+ ions*. The theoretical DR rate obtained for H_2D^+ and D_2H^+ in the present study is in a good agreement with the three different storage-ring experiments: CRYRING [35], TARN II [10], and TSR [57]. The main disagreement to mention is that the theoretical DR rate shows few dips at that are not presented in the experimental DR rate. The second important disagreement is in the low-energy region for D_2H^+, where theory DR is below the experiment by a factor of 3–4. The reason for these disagreements is unknown.

In conclusion, we have developed a theoretical method for treatment of the dissociative recombination in triatomic C_{2v} molecular ions. We applied the method to interpretation of DR experiments with the H_2D^+ and D_2H^+. The theoretical rate obtained is in reasonably good agreement with the experiments, overall, but with some notable discrepancies that may eventually prove to be informative for theory, and possibly for the experiments as well.

ACKNOWLEDGMENTS

This work has been supported by the National Science Foundation under Grant No. PHY-0427460 and Grant No. PHY-0427376, by an allocation of NERSC supercomputing resources, and by an allocation of NCSA supercomputing resources (Project No. PHY040022). The authors are grateful to A. Wolf for fruitful discussions.

APPENDIX

There are three distributions that must be considered: (1) the collision energy distribution, (2) the rotational energy distribution, and (3) the toroidal correction.

1. Convolution over the distribution of collision energies

One distribution $f(E_x,E_y,E_z)$ is over the relative energy of colliding H_3^+ and e^-. In the storage-ring experiments [11,13,31,57], $f(E_x,E_y,E_z)$ is not isotropic: the width of the distribution along one spatial direction (let it be the x component $E_x=E_\parallel$) differs from the widths along the other two directions (E_y and E_z). The widths along y and z are the same. For the sum E_y+E_z we will use the symbol $E_\perp$. Let the corresponding widths be $\Delta E_\parallel$ and $\Delta E_\perp$. We need to consider velocities v_i as well as energies E_i, $i=x,y,z$. The total velocity of the electron relative to the ion is $\vec{v}=\vec{v}_\parallel+\vec{u}$, where $v_\parallel$ is the velocity measured in the experiment. This velocity is the center of the velocity distribution. $\vec{u}$ is the velocity that describes the distribution; it represents the deviation of the total velocity from the center of the distribution. We also represent $\vec{u}$ as a sum of two contributions $\vec{u}=\vec{u}_\perp+\vec{u}_\parallel$, assuming that $\vec{u}_\parallel$ and $\vec{v}_\parallel$ are collinear. Then, the averaging over the nonisotropic distribution $f(E_x,E_y,E_z)$ is carried out through the integral

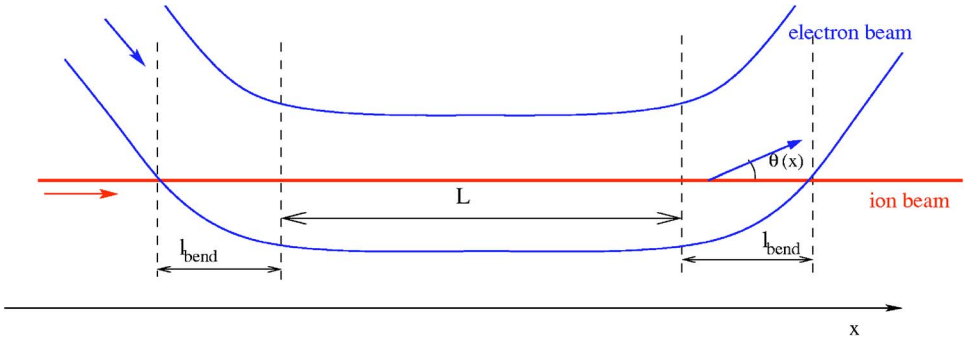

FIG. 5. (Color online) From Ref. [34]. Geometry of the toroidal effect in storage-ring experiments, showing how the ion and electron beams are not parallel at the interaction region edges.

$$\langle \alpha(v_\parallel) \rangle = \frac{1}{C} \int d^3u \exp\left(-\frac{u_\perp^2}{2\Delta E_\perp}\right) \times \exp\left(-\frac{u_\parallel^2}{2\Delta E_\parallel}\right) \alpha(|\vec{v}_\parallel + \vec{u}_\perp + \vec{u}_\parallel|), \quad \text{(A1)}$$

where C is the normalization constant:

$$C = \int d^3u \exp\left(-\frac{u_\perp^2}{2\Delta E_\perp}\right) \exp\left(-\frac{u_\parallel^2}{2\Delta E_\parallel}\right) = (2\pi)^{3/2} E_\perp \sqrt{\Delta E_\parallel}. \quad \text{(A2)}$$

Switching from velocity $u_\perp$ to energy $E_\perp$ in Eq. (A1), we have

$$\langle \alpha(v_\parallel) \rangle = \frac{1}{(2\pi)^{1/2} E_\perp \sqrt{\Delta E_\parallel}} \int_{-\infty}^{\infty} du_\parallel \exp\left(-\frac{u_\parallel^2}{2\Delta E_\parallel}\right) \times \int_0^\infty dE_\perp \exp\left(-\frac{E_\perp}{\Delta E_\perp}\right) \alpha[(v_\parallel + u_\parallel)^2/2 + E_\perp]. \quad \text{(A3)}$$

2. Rotational energy averaging

In addition to the relative velocity distribution, in the experiment there is a non-negligible population of different rotational energy levels associated with the rotation of the ion. It is reasonable to assume that such a distribution obeys Boltzmann statistics. Therefore, the DR rate calculated for different initial rotational states of H_3^+ should be weighted with the factor $\exp[-(E_{rot}-E_0)/kT_{rot}]$, where E_{rot} is the energy of a given rotational level contributing to the total DR rate and E_0 is the lowest rotational states among all rotational states. The additional averaging takes the form

$$\frac{1}{C_{rot}} \sum_{rot} (2I+1)(2N^+ + 1) \exp\left(-\frac{E_{rot}-E_0}{kT_{rot}}\right) \alpha_{rot},$$

with the normalization constant C_{rot}:

$$C_{rot} = \sum_{rot} (2I+1)(2N^+ + 1) \exp\left(-\frac{E_{rot}-E_0}{kT_{rot}}\right).$$

In the above formula we include the statistical factor $(2I+1)(2N^+ + 1)$ that accounts for the $(2I+1)$ degenerate projections of the nuclear spin ($I=1/2$ or $3/2$ for H_3^+) and the $(2N^+ + 1)$ projections of the ionic angular momentum on a space-fixed axis. Therefore, the full averaging procedure is given by the following formula:

$$\langle \alpha(v) \rangle = \frac{1}{(2\pi)^{1/2} E_\perp \sqrt{\Delta E_\parallel} C_{rot}} \sum_{rot} (2I+1)(2N^+ + 1) \times \exp\left(-\frac{E_{rot}-E_0}{kT_{rot}}\right) \int_{-\infty}^{\infty} du_\parallel \exp\left(-\frac{u_\parallel^2}{2\Delta E_\parallel}\right) \int_0^\infty dE_\perp \times \exp\left(-\frac{E_\perp}{\Delta E_\perp}\right) \alpha_{rot}[(v_\parallel + u_\parallel)^2/2 + E_\perp]. \quad \text{(A4)}$$

3. Toroidal correction

There is one more experimental factor that has not yet been described in the theoretical description presented above: the so-called toroidal correction. (The toroidal correction was not included in our previous work [29,30], but it was addressed briefly in Ref. [34].)

The electron-ion interaction region in a storage ring experiment actually consists of two different regions (see Fig. 5): the region p of length L, where the electron and ion beams are parallel, and two symmetric regions of length l_{bend} each, where the electrons are bent into and out of the ion beam (region b).

Experimentally, the dissociative recombination rate $\alpha_{meas}(E)$ is determined from the measured number of dissociative recombination events K_{DR} that occur per unit time interval,

$$K_{DR} = \alpha_{meas}(E) n_e n_i A L. \quad \text{(A5)}$$

Here n_i and n_e are, respectively, the ion and electron densities, L is the length of the interaction region, and A is the cross-section area of the ion beam (assumed here to be smaller than the electron beam cross-sectional area). In the formula above, $\alpha_{meas}(E) n_e$ represents a probability per second for one ion to dissociate and the value $n_i AL$ gives the total number of ions in the interaction region. In the analysis of experimental data, L is taken as the length of the parallel portion of the interaction region. Since the relative velocity of electrons with respect to ions is not exactly uniform along the interaction region, especially at its edges, $\alpha_{meas}(E)$ represents an average of the actual DR rate $\alpha(E)$ over a range of relative electron-ion energies E. The relation between $\alpha(E)$ and $\alpha_{meas}(E)$ can be found by first writing down the rate of DR events dK_{DR} that occur within a small portion dx of the interaction region:

$$dK_{DR} = \alpha(\tilde{E}(x))n_e n_i A dx. \quad \text{(A6)}$$

Consequently, for the rate K_{DR} we obtain

$$K_{DR} = \int_{int.region} \alpha(\tilde{E}(x))n_e n_i A dx, \quad \text{(A7)}$$

where the notation $\tilde{E}(x)$ reflects the fact that the relative kinetic energy $\tilde{E}$ depends on the position x in the bending region b. This gives the following expression for $\alpha_{meas}(E)$:

$$\alpha_{meas}(E) = \frac{1}{L}\int_{int.region} \alpha(\tilde{E}(x))dx. \quad \text{(A8)}$$

Since in the central region the ion and electron beams are parallel, the integral can be written as

$$\alpha_{meas}(E) = \alpha(E) + \frac{2}{L}\int_0^{l_{bend}} \alpha(\tilde{E}(x))dx. \quad \text{(A9)}$$

The last integral needs to be evaluated only for one of the two symmetric regions, where the beams are not parallel. The energy E on the left-hand side of Eq. (A9) refers to the relative energy in the region p. The relative energy $\tilde{E}(x)$ can be calculated from E and from the known dependence of the angle $\theta(x)$ between ionic and electron velocities as a function of x. The angle $\theta(x)$ in the bending region has been measured experimentally. Using the vector addition rule we find (in atomic units)

$$\tilde{E}(x) = \tilde{E}(x(\theta)) = E + m_{ion}v_i v_e(1 - \cos\,\theta). \quad \text{(A10)}$$

The ion velocity v_i is determined from the frequency f of the storage ring revolution and the length S of the ion path within the storage ring: $v_i = fS$. The electron velocity is obtained from v_i and any given relative kinetic energy E in the region p:

$$v_e = v_i \pm \sqrt{2E}. \quad \text{(A11)}$$

The sign ± means that the electron velocity can be larger or smaller than the ion velocity.

Evaluating the integral (A9) for H_3^+, we have used the following parameters, taken from Ref. [58]:

$$f = 539730\ \text{s}^{-1},$$

$$S = 51.6\ \text{m},$$

$$\theta(x) = A_2\left(1 - \frac{1}{1 + (x/x_0)^p}\right),$$

$$p = 2.35271, \quad A_2 = 0.75638\ \text{rad}, \quad x_0 = 313.776\ \text{mm},$$

$$l_{bend} = 255\ \text{mm},$$

$$L = 850\ \text{mm}. \quad \text{(A12)}$$

To combine the toroidal correction effect with the theoretical DR rate, to simulate the experimental conditions, we took our calculated DR rate, convolved it with the experimental rotational E_{rot}, transverse $E_\perp$, and parallel $E_\parallel$ energy distributions. In order to include the toroidal correction properly, we need the higher-energy DR rate above 2 eV, where we have not performed calculations. To this end, we have smoothly joined our theoretical curve below 2 eV with the experimental data above 3.8 eV. We use this dependence as $\alpha(\tilde{E})$ in Eqs. (A8) and (A9). The result of this calculation is the effective experimental DR rate coefficient. For H_3^+, it is shown in Fig. 6.

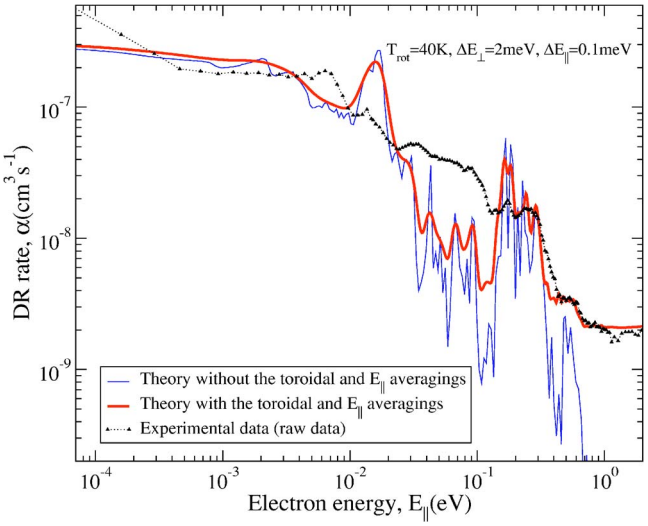

FIG. 6. (Color online) Experimental [13] (triangles) and theoretical (two solid lines) H_3^+ DR rates. The thick line represents the theoretical rate averaged according to Eqs. (A3), (A4), and (A9). The thin line represents the result published in our previous work [29,30], where the averaging over $\Delta E_\parallel$ and the toroidal averaging were not performed. Clearly, the $\Delta E_\parallel$ averaging and the toroidal correction are both very important.

The inclusion of the toroidal effect significantly changes the measured DR rate in a storage ring experiment, particularly in energy regions where the DR rate is small. One example is the 0.4–2 eV region in Fig. 6, where the DR rate with the toroidal effect is much higher than the rate without it. In some storage-ring experiments there were attempts to make an iterative deconvolution—i.e., an inversion of the integral in Eq. (A9). Such a deconvolution may produce results with large error bars in energy regions where the DR rate is small, if the full, energy-dependent DR rate is not known in advance. For this reason, we believe that a better test of the theory is achieved by directly comparing the measured rates with a theoretical simulation that incorporates the experimental details.

When we published our initial theoretical work [29,30] on H_3^+, we were not familiar with all of these experimental conditions and the relevant averaging procedures needed to fully describe the measured recombination rates. For completeness we provide here in Fig. 6 the theoretical H_3^+ DR rate that includes all such averaging aspects. This figure shows that the averaging significantly improves the agreement between theory and experiment. For example, the toroidal correction gives almost perfect agreement at the higher

end of the energy range that we have calculated (0.4–2 eV), although the measured DR events in this region are predominantly sampling the energies above 2 eV through the toroidal effect. The averaging over $\Delta E_{\|}$ smears out many deep resonances in the theoretical rate, which are not visible in the experimental DR rate at the present day experimental resolution but which could in principle be measured in the future as experimental capabilities improve.

[1] T. R. Geballe and T. Oka, Nature (London) **384**, 334 (1996).
[2] T. R. Geballe, B. J. McCall, K. H. Hinkle, and T. Oka, Astrophys. J. **510**, 251 (1999).
[3] B. J. McCall and T. Oka, Science **287**, 1941 (2000).
[4] T. R. Geballe, Philos. Trans. R. Soc. London, Ser. A **358**, 2503 (2000).
[5] F. Scappini, C. Cecchi-Pestellini, C. Codella, and A. Dalgarno, Mon. Not. R. Astron. Soc. **317**, L6 (2000).
[6] T. Oka, Philos. Trans. R. Soc. London, Ser. A **358**, 2363 (2000).
[7] B. J. McCall, Ph.D. thesis, University of Chicago, 2001.
[8] M. Larsson, H. Danared, J. R. Mowat, P. Sigray, G. Sundström, L. Broström, A. Filevich, A. Källberg, S. Mannervik, K. G. Rensfelt, and S. Datz, Phys. Rev. Lett. **70**, 430 (1993).
[9] G. Sundström, J. R. Mowat, H. Danared, S. Datz, L. Broström, A. Filevich, A. Källberg, S. Mannervik, K. G. Rensfelt, P. Sigray, M. af Ugllas, and M. Larsson, Science **263**, 785 (1994).
[10] T. Tanabe, I. Katayama, H. Kamegaya, K. Chida, Y. Arakaki, T. Watanabe, M. Yoshizawa, M. Saito, Y. Haruyama, K. Hosono, K. Hatanaka, T. Honma, K. Noda, S. Ohtani, and H. Takagi, in *Dissociative Recombination: Theory, Experiment and Applications III*, edited by D. Zaifman, J. B. A. Mitchell, D. Schwalm, and B. R. Rowe (World Scientific, Singapore, 1996), p. 84.
[11] M. Larsson, Philos. Trans. R. Soc. London, Ser. A **358**, 2433 (2000).
[12] T. Tanabe, K. Chida, T. Watanabe, Y. Arakaki, H. Takagi, I. Katayama, Y. Haruyama, M. Saito, I. Nomura, T. Honma, K. Noda, and K. Hoson, in *Dissociative Recombination: Theory, Experiment and Applications IV*, edited by M. Larsson, J. B. A. Mitchell, and I. F. Schneider (World Scientific, Singapore, 2000), p. 170.
[13] B. J. McCall, A. J. Huneycutt, R. J. Saykally, T. R. Geballe, N. Djuric, G. H. Dunn, J. Semaniak, O. Novotny, A. Al-Khalili, A. Ehlerding, F. Hellberg, S. Kalhori, A. Neau, R. Thomas, F. Österdahl, and M. Larsson, Nature (London) **422**, 500 (2003).
[14] L. Lammich, D. Strasser, H. Kreckel, M. Lange, H. B. Pedersen, S. Altevogt, V. Andrianarijaona, H. Buhr, O. Heber, P. Witte, D. Schwalm, A. Wolf, and D. Zajfman, Phys. Rev. Lett. **91**, 143201 (2003).
[15] A. P. Hickman, J. Phys. B **20**, 2091 (1987).
[16] A. Giusti, J. Phys. B **13**, 3867 (1980).
[17] A. Giusti-Suzor, J. N. Bardsley, and C. Derkits, Phys. Rev. A **28**, 682 (1983).
[18] A. Giusti-Suzor and Ch. Jungen, J. Chem. Phys. **80**, 986 (1984).
[19] K. Nakashima, H. Takagi, and H. Nakamura, J. Chem. Phys. **86**, 726 (1987).
[20] Ch. Jungen and S. C. Ross, Phys. Rev. A **55**, R2503 (1997).
[21] M. G. Golubkov, G. V. Golubkov, and G. K. Ivanov, J. Phys. B **30**, 5511 (1997).
[22] I. F. Schneider, C. Stromholm, L. Carata, X. Urbain, M. Larsson, and A. Suzor-Weiner, J. Phys. B **30**, 2687 (1997).
[23] E. S. Chang and U. Fano, Phys. Rev. A **6**, 173 (1972).
[24] C. H. Greene and Ch. Jungen, Adv. At. Mol. Phys. **21**, 51 (1985).
[25] M. Aymar, C. H. Greene, and E. Luc-Koenig, Rev. Mod. Phys. **68**, 1015 (1996).
[26] Ch. Jungen, *Molecular Applications of Quantum Defect Theory* (Institute of Physics, Bristol, 1996).
[27] A. E. Orel and K. C. Kulander, Phys. Rev. Lett. **71**, 4315 (1993).
[28] I. F. Schneider, A. E. Orel, and A. Suzor-Weiner, Phys. Rev. Lett. **85**, 3785 (2000).
[29] V. Kokoouline and C. H. Greene, Phys. Rev. Lett. **90**, 133201 (2003).
[30] V. Kokoouline and C. H. Greene, Phys. Rev. A **68**, 012703 (2003).
[31] M. J. Jensen, H. B. Pedersen, C. P. Safvan, K. Seiersen, X. Urbain, and L. H. Andersen, Phys. Rev. A **63**, 052701 (2001).
[32] V. Kokoouline, C. H. Greene, and B. D. Esry, Nature (London) **412**, 891 (2001).
[33] A. E. Orel, I. F. Schneider, and A. Suzor-Weiner, Philos. Trans. R. Soc. London, Ser. A **358**, 2445 (2000).
[34] V. Kokoouline and C. H. Greene, J. Phys.: Confer. Ser. **4**, 74 (2005).
[35] M. Larsson, H. Danared, A. Larson, A. Le Padellec, J. R. Peterson, S. Rosen, J. Semaniak, and C. Strömholm, Phys. Rev. Lett. **79**, 395 (1997).
[36] W. Cencek, J. Rychlewski, R. Jaquet, and W. Kutzelnigg, J. Chem. Phys. **108**, 2831 (1998).
[37] R. Jaquet, W. Cencek, W. Kutzelnigg, and J. Rychlewski, J. Chem. Phys. **108**, 2837 (1998).
[38] V. Kokoouline and C. H. Greene, Faraday Discuss. **127**, 413 (2004).
[39] P. Bunker and P. Jensen, *Molecular Symmetry and Spectroscopy* (NRC Research Press, Ottawa, 1998).
[40] U. Fano, Phys. Rev. A **2**, 353 (1970).
[41] U. Fano and K. T. Lu, Can. J. Phys. **62**, 1264 (1984).
[42] S. H. Pan and K. T. Lu, Phys. Rev. A **37**, 299 (1988).
[43] J. A. Stephens and C. H. Greene, Phys. Rev. Lett. **72**, 1624 (1994).
[44] J. A. Stephens and C. H. Greene, J. Chem. Phys. **102**, 1579 (1995).
[45] H. C. Longuet-Higgins, *Advances in Spectroscopy* (Interscience, New York, 1961), Vol. II, p. 429.
[46] A. Staib, W. Domcke, and A. Sobolewski, Z. Phys. D: At., Mol. Clusters **16**, 49 (1990).
[47] A. Staib and W. Domcke, Z. Phys. D: At., Mol. Clusters **16**, 275 (1990).
[48] B. R. Johnson, J. Chem. Phys. **73**, 5051 (1980).

[49] J. H. Macek, J. Phys. B **1**, 831 (1968).
[50] E. Cuervo-Reyes, J. Rubayo-Soneira, A. Aguado, M. Paniagua, C. Tablero, C. Sanz, and O. Roncero, Phys. Chem. Chem. Phys. **4**, 6012 (2002).
[51] O. L. Polyansky and J. Tennyson, J. Chem. Phys. **110**, 5056 (1999).
[52] O. I. Tolstikhin, S. Watanabe, and M. Matsuzawa, J. Phys. B **29**, L389 (1996).
[53] O. I. Tolstikhin, V. N. Ostrovsky, and H. Nakamura, Phys. Rev. Lett. **79**, 2026 (1997).
[54] O. I. Tolstikhin, V. N. Ostrovsky, and H. Nakamura, Phys. Rev. A **58**, 2077 (1998).
[55] A. Vibok and G. G. Balint-Kurti, J. Chem. Phys. **96**, 8712 (1992).
[56] A. Vibok and G. G. Balint-Kurti, J. Phys. Chem. **96**, 7615 (1992).
[57] L. Lammich, D. Strasser, H. Kreckel, M. Lange, H. B. Pedersen, S. Altevogt, V. Andrianarijaona, H. Buhr, O. Heber, P. Witte, D. Schwalm, A. Wolf, and D. Zajfman, Phys. Rev. Lett. **91**, 143201 (2003).
[58] Å. Larson (private communication).